Sains Malaysiana 54(3)(2025): 943-958
http://doi.org/10.17576/jsm-2025-5403-24

Dosimetric Evaluation of 3D-Printed Polylactic Acid (PLA) Anthropomorphic Radiotherapy Head Phantom using Gafchromic EBT-XD Films, OSLD NanoDot and TLD-100

(Penilaian Dosimetrik Kepala Fantom Radioterapi Antropomorfik Asid Polilaktik Bercetak 3D (PLA) menggunakan Filem Gafchromic EBT-XD, OSLD NanoDot dan TLD-100)

NOOR NABILAH TALIK SISIN[1,7], NUR EMIRAH MOHD ZAIN[2], NOR ARINA ISAMAIL[2], REDUAN ABDULLAH[3], MUHAMMAD AFIQ KHAIRIL ANUAR[4], NUR HAMIZAH MOHD ZAINUDIN[5], AHMAD BAZLIE ABDUL KADIR[6], ASHRANI AIZZUDDIN ABD RAHNI[8], WAN NORDIANA RAHMAN[1,7,*], AML ALMUTERY[1,9] & RAIZULNASUHA ABD RASHID[10]

[1]Department of Applied Physics, Universiti Kebangsaan Malaysia, 43600 UKM Bangi, Selangor, Malaysia
[2]School of Health Sciences, Universiti Sains Malaysia, Kubang Kerian, Kelantan, Malaysia
[3]Oncology, Radiotherapy and Nuclear Medicine Department, Hospital Universiti Sains Malaysia, 16150 Kubang Kerian, Kelantan, Malaysia
[4]Department of Health Professional, Faculty of Health Science, Management & Science University, 40100 Shah Alam, Selangor, Malaysia
[5]Faculty of Health Sciences, Universiti Sultan Zainal Abidin, Gong Badak Campus, 21300 Kuala Terengganu, Terengganu Malaysia
[6]Department of Metrology, Nuclear Malaysia Agency, 43000 Bangi, Selangor, Malaysia
[7]Nuclear Technology Research Centre, Faculty of Science and Technology, Universiti Kebangsaan Malaysia, 43600 UKM Bangi, Selangor, Malaysia
[8]Department of Electrical, Electronic and Systems Engineering, Faculty of Engineering and Built Environment, Universiti Kebangsaan Malaysia, 43600 UKM Bangi, Selangor, Malaysia
[9]Physics Department, Faculty of Science and Humanities in Ad-Dawadmi, Shaqra University, Shaqra 11911, Saudi Arabia
[10]Centre for Diagnostic Nuclear Imaging, Universiti Putra Malaysia, 43400 UPM Serdang, Selangor, Malaysia

Received: 18 August 2024/Accepted: 28 November 2024

ABSTRACT

Recently, additive manufacturing or 3-dimensional (3D) printing has been utilized to create low-cost and customized radiotherapy phantoms for quality assurance and radiation dosimetry. In this study, the head phantom was fabricated by scanning a standard RANDO® head phantom using a Kinect® Xbox 360® and printed using polylactic acid (PLA) with 100% infill. The 3D-printed anthropomorphic head phantoms underwent CT simulation, treatment planning, and treatment delivery, similar to the patient setup in radiotherapy with a whole brain target. Irradiation of the phantoms were delivered with a single fraction of 400 cGy using 6 MV photon beam energy. The absorbed dose was measured with three dosimeters: GafChromic EBT-XD film, TLD-100, and OSLD NanoDot. Gamma analysis of EBT-XD films indicated a 30% dose difference for the irradiation's pass rate of 3D printed head phantom and RANDO® phantom compare to TPS dose calculation. TLD's measurement of the 3D printed phantom resulted in 99% similarity to the TPS calculation and RANDO® phantom TLD's results. Meanwhile, the percentage dose difference between OSLD reading of 3D printed phantom and TPS calculation was 8.1%. Therefore, this study demonstrates the feasibility of the 3D-printed head RP as an alternative phantom to RANDO® head RP. Further improvement in the phantom design details might enhance the dosimetry outcome and accuracy.

Keywords: Anthropomorphic; EBT; PLA; OSLD; TLD; 3D printing

ABSTRAK

Mutakhir ini, proses pembuatan bahan tambahan atau lebih dikenali sebagai percetakan 3D telah diaplikasikan dalam penghasilan fantom radioterapi berkos rendah untuk tujuan jaminan kualiti dan dosimetri radiasi. Dalam penyelidikan ini, fabrikasi model kepala fantom telah dilakukan berpandu kepada model kepala fantom RANDO® mengunakan Kinect® Xbox 360® dan dicetak menggunakan bahan polilaktik asid (PLA) dengan pengisian 100%. Model percetakan

3D antropomorfik kepala fantom yang dihasilkan akan melalui proses simulasi CT, perancangan rawatan, penghantaran rawatan yang serupa seperti mana rawatan kepada pesakit dengan sasaran tertumpu kepada keseluruhan otak. Penyinaran fantom telah dilakukan dengan pecahan tunggal 400 cGy menggunakan tenaga pancaran foton 6 MV. Dos terserap diukur dengan menggunakan tiga jenis dosimeter iaitu filem *GafChromic EBT-XD, TLD-100* dan *OSLD NanoDot*. Analisis indeks Gamma menggunakan filem *GafChromic EBT-XD* menunjukkan 30% perbezaan dos bagi kadar radiasi yang dibenarkan untuk fantom percetakan 3D dan fantom RANDO® dengan pengiraan dos TPS. Manakala pengukuran TLD menunjukkan keputusan 99% kebersamaan dengan pengiraan TPS bagi perbandingan dengan fantom RANDO®. Sementara itu perbezaan dos antara bacaan OSLD bagi fantom percetakan 3D dan TPS adalah sebanyak 8.1%. Oleh itu, kajian ini telah menunjukkan kebolehlaksanaan fantom percetakan 3D sebagai alternatif kepada fantom radioterapi kepala RANDO®. Penambahbaikan reka bentuk secara lebih terperinci boleh meningkatkan hasil dan ketepatan dosimetri.

Kata kunci: Antropomofik; EBT; OSLD; percetakan 3D; PLA; TLD

INTRODUCTION

Radiotherapy is one of the critical types of cancer treatment other than chemotherapy and surgery. It uses ionizing radiation to destroy cancer cells and suppress cancer cell growth. Treatment planning before radiotherapy is crucial to deliver sufficient doses to the patients. For the treatment to be successful, thorough studies on dosimetry are vital to ensure the efficiency and accuracy of the radiation dose during treatment (Attix 2004; DeWerd & Kissick 2014; Frigo 2014; Niroomand-Rad et al. 1998; Tagiling 2019).

After the cancer diagnosis and treatment consent from physicians, patients would have to undergo body radiographic imaging using several options such as dynamic contrast-enhanced computed tomography (CT), X-ray simulator, positron emission tomography (PET), or multi-parametric magnetic resonance imaging (MRI) (Hoskin & Alonzi 2016), to localize the tumor and identify patient's positioning for treatment administration. The CT images are used for treatment planning procedures such as organ contouring, beam insertion, and radiation dose prescription (Bogmis et al. 2020; Piperdi et al. 2021). During the treatment verification and planning, a radiotherapy phantom (RP) is employed and set up just like a genuine patient for re-simulation. Radiotherapy will be conducted on the patient when the treatment planning is verified.

The RP is an object that could simulate the properties of the human body's material (Ahmad et al. 2021) and can replace the patients during radiation dosimetry (Zain et al. 2019). Commercial human-body-like phantoms such as Alderson RANDO® RP (The Phantom Laboratory, Salem, NY, USA) are made of materials mimicking the different densities in the human body (tissue-equivalent) (Park et al. 2017). Theoretically, the materials of choice for phantom must be a tissue or water equivalent that poses similar effective atomic number, number of electrons per unit gram, and mass density (Khan 2014). These aspects suit the Compton scattering effect as it was the most prominent interaction type in radiotherapy's clinical energy range of megavoltage beams (Khan 2014).

Unfortunately, the RANDO® RP is very costly in production and only obtainable in a standard healthy person size, compared to the actual variation of an unhealthy patient body. These issues lead to dosimetric errors as the phantom does not mimic actual patients. A slight disparity between the phantoms and patients' organs would generate a dosimetry error (Burleson et al. 2015). Other current phantoms are designed to be tissue equivalent, but most do not mimic 100% of the human body's inhomogeneity and density. In addition, there is a more advanced patient-specific phantom, but it involves complex and costly productions. The implementation of 3D printing technology also enabling efficient workflow that is time saving without delaying treatment planning process (Tino et al. 2022).

Nowadays, researchers have found that RPs' production through additive manufacturing or 3-dimensional (3D) printing is economical and uncomplicated (Babaloui et al. 2020). The 3D-printed RPs could be created using a custom-made approach and personalized shapes (Bustillo, Tumlos & Remoto 2019; Craft & Howell 2017; Oh et al. 2017; Zain et al. 2019). The materials applied in 3D printing technology could vary in their properties, strength, durability, flexibility, heat resistance, biocompatibility, and biodegradability (Alssabbagh et al. 2017; Kairn, Crowe & Markwell 2015; Zhang et al. 2019). Among the water-equivalent materials that are being utilized for anthropomorphic RPs are acrylonitrile butadiene styrene (ABS) (Ahmad et al. 2021), polylactic acid (PLA) (Ahmad et al. 2021; Craft & Howell 2017), thermoplastic polyurethane (TPU) (Rahman et al. 2023) solid acrylic plastic (Gear et al. 2016), polystyrene-solid water with acrylic (Molineu et al. 2005), polymethyl-methacrylate (PMMA) (Mann et al. 2017), or resin-based materials (Dawood et al. 2015). According a research survey, PLA is the most popular used material for 3D printed phantoms for radiotherapy in United Kingdom (Sands et al. 2023).

Several teams have worked on the 3D-printed head and neck anthropomorphic RPs fabrications. Some researchers produced phantoms with different materials for the shells and inside infills, such as polystyrene insert block (Molineu et al. 2013. 2005), acrylic shell, Clear Ballistic gel and Superflab (Steinmann et al. 2020), ABS and M3 mix (Ehler et al. 2014), as well as ABS and PLA

(Ahmadi et al. 2021). There are also H&N RPs that were entirely produced using Perspex material (Radaideh et al. 2013), radiopaque printed paper sheets (Jahnke et al. 2019), and PLA (Kadoya et al. 2019; Kamomae et al. 2017). Nevertheless, Kamomae's and Kadoya's teams were only able to fabricate a 3-cm slice phantom (not a whole head RP) produced from patient's CT images. Recently, 3D printing technology have been applied in more advanced technique in radiotherapy. 3D printed stereotactic radiosurgery quality assurance phantom have been fabricated for single plan techniques of complexed multiple brain targets (MBT) (Mukwada et al. 2024). 3D printing also have been used to develop anthropomorphic phantom to optimize cone beam computed tomography (CBCT) protocols for head and neck (H&N) radiotherapy treatments (Alzahrani et al. 2024). 3D printed phantom purposes has evolved into assisting precise patient positioning and optimising imaging protocol that will help to reduce the patient's dose (Alzahrani et al. 2024). Bustillo et al. (2024) have fabricated heterogeneous paediatric head and thorax phantoms useful in clinical radiotherapy quality assurance. Their study shows that 3D printed phantoms are effective equipment in doing clinical dosimetry and educational training. This paper shows that 3D printing are very useful and capable to be used for clinical purposed. Feasibility of a treatment and imaging technique at preclinical level also require vigorous study to be translated into clinical. Therefore, 3D printing technique is an important technique that will boost preclinical and experimental study in radiotherapy. Phantom are normally available for clinical application but for preclinical work, the specific phantom need to be customize especially with studies involved animal and cell culture models. One of the preclinical dosimetry setups that have been investigated is the development of phantom for FLASH radiotherapy using synchrotron radiation where a customize phantom are required due to the unique set up in the synchrotron beamline (Bustillo et al. 2024).

The current study presents a development process of a 3D-printed anthropomorphic whole-head RP with previously evaluated PLA material (Zain et al. 2019). Microsoft® Kinect® Xbox 360® scanner was utilized to obtain superficial anatomical features, which is easily accessible with no radiation compared to a CT simulator (Zain & Rahman 2020). The dosimetric characterization of the 3D-printed head RP was conducted with GafChromic™ EBT-XD films, thermoluminescence dosimeter (TLD-100), and NanoDot optically stimulated luminescence dosimeter (OSLD).

MATERIALS AND METHODS

3D-PRINTED HEAD RP DESIGN

3D Scanning

The RANDO® RP was scanned using a Microsoft® Kinect® Xbox 360° scanner (Microsoft® Corporation, Albuquerque, Mexico) and Skanect software (Microsoft® Corporation, Albuquerque, Mexico) following the previously published procedures (Zain & Rahman 2020). The scanner-to-phantom distance was set to 50 cm, and the scanner angle was adjusted to be within 10°. The Skanect software covered the geometric form of the prototype head phantom, and the RANDO® RP was rotated in its isocenter. The Kinect scanner was fixed at a static position, as slight movements would disrupt its infrared sensitivity (Rahman 2017; Ramos 2012).

3D Editing

The 3D scanned image of the phantom was further edited. Smoothing an external surface of the head phantom and removing the unwanted parts were completed using the scanning program Skanect software. The scanned results of meshes were accomplished in very high image data up to hundreds of millions of faces and thousands of edges. Hence, it needs to be reduced to a lower number of faces (less than a hundred thousand) to be exported to the 3D editing software. Filling apertures and building the image data in the watertight mode were run during the editing process. The steps of editing are (1) the watertight process, (2) the move and cropped process, and (3) the removal of unwanted parts.

Rendering and smoothing of the images continued using 3D Builder (Microsoft® Corporation, Albuquerque, Mexico) and Sculptris (Autodesk Inc., San Rafael, CA, USA) software. The designs of phantom slices and dosimeter insertion slots were designed using Blender (Blender Foundation, Amsterdam, Netherlands) software. The image of the original whole-head phantom model was sliced into ten slices with 2.5 cm sagittal thickness, as shown in Figure 1(A) and 1(B). The dosimeter slots were designed according to the positions of the dosimeter slots in RANDO® RP as depicted in Figure 1(C) and Figure 1(D). Figure 1(E) shows the final design of 3D printed phantom.

3D-PRINTED HEAD RP DEVELOPMENT

3D printing

After completing the 3D editing of the phantom image, the data from the editing software were saved in 3D mesh in stereolithography (STL) format. The printing process was conducted using Cura (Ultimaker, Netherlands) software, which is a 3D application that is compatible with the STL file. The phantom was designed as a 100% solid object as it is sturdier and more robust.

The fused deposition modeling (FDM) technique was employed using the 3D printer (MyVista Cube 200 Machine) with 30 mm/s print speed, 30 mm/s travel speed, 0.1 mm layer height, 200 ºC operating temperature, 0.4 mm nozzle diameter, and the density fill is 100%. The material used in the current work is PLA (Zain et al. 2019). The manufacturing of the filament starts with unrefined and powder-state resin that is transparent in color. The process

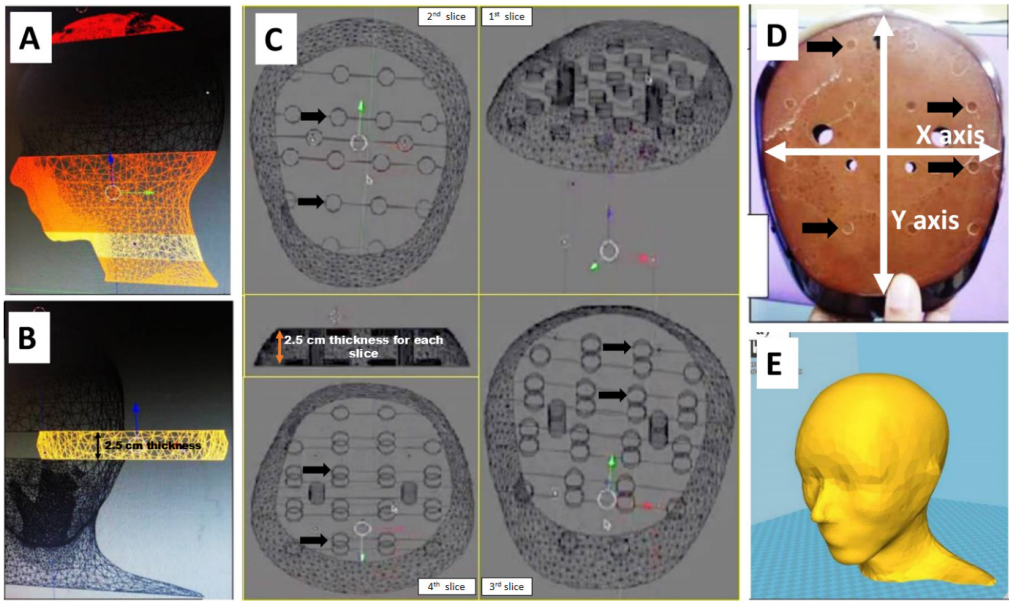

FIGURE 1. 3D editing processes. (A-B) Cropping process of the 3D image of the head phantom, (C) The slots editing process, (D) A RANDO®'s slice with slots (black arrows), showing the geometric measurement of the phantom with X- and Y-axis values, and (E) The 3D image before final slices 3D printing

continues with the mixture of that resin with additional pigment that leads to a purple color. Next, the mixture underwent heating and cooling and was finally thrust into a solid PLA filament.

Geometric Evaluations

Each phantom slice was measured manually using a standard ruler based on X- and Y-axis values, as illustrated in Figure 1(D). The reading was taken three times, and the average values of X and Y for each slice for both RANDO® RP and 3D-printed RPs were then calculated. The weight between the two phantoms was also measured using the weighting platform scale device.

DOSIMETRIC CHARACTERIZATION OF 3D-PRINTED HEAD RP

CT Simulation

A Brilliance Big Bore Computed Tomography (CT) simulator (Phillips Healthcare, Andover, MA, USA) is employed to analyze the Hounsfield Unit (HU) and internal uniformity of both the RANDO® RP and 3D-printed RP. The CT simulation was carried out at the Nuclear Medicine, Radiotherapy, and Oncology Department, Hospital Universiti Sains Malaysia.

The positioning of the simulation started by aligning the phantom according to the three lasers intersecting at the middle, left, and right lateral. During positioning, immobilization devices such as head-rest B and 2 cm-poly are used. The three intersections represent the location of the isocentre of the phantom. The isocentre was positioned in the middle of the two eyes at a depth of ± 0.2 cm since the targeted area was a whole brain. Next, the three-laser intersection was marked using a marker as a reference during irradiation using Primus linear accelerator (LINAC) (Siemens, Big-bore Computed Tomography, CT scan). Afterward, 3D images of both phantoms in topography data were obtained.

The parameter setup on the CT simulation was as follows: slice thickness: 3 cm, peak voltage: 120 kVp, current: 300 mAs, window width: 375, window level: 40, and field of view: -268.60 mm and 604 mm. Three regions of interest (ROI) were drawn for all slices from the CT images. In addition, the average HU number is calculated for every slice. After the simulation, the obtained topography images and data were imported to a treatment planning system (TPS) in DICOM (Digital Imaging and Communicating in Medicine) format for the treatment delivery planning.

Treatment Planning

After the CT simulation, all the image datasets were imported into the Nucletron Oncentra Planning System 4.3 TPS. Image registration was executed by contouring the organs at risk (Niroomand-Rad et al. 1998), which are the skin, left and right eyes, left and right optic nerves, and spinal cord, as well as the target area, which is the brain. After-image registration, the beams were inserted

into the planning through the plan manager segment, and the treatment was planned based on the H&N treatment. Two opposite-field beams were inserted separately into the planning at 90° and 270°. Isocentre placement was based on the mark constructed during the simulation process. It was located between eyes within 0.2 cm depth with standard values of the x-axis, y-axis, and z-axis, which were 0.2 cm, -2.1 cm, and -4.13 cm, respectively. The prescribed dose was 20 Gy with five fractions, hence 400 cGy per fraction. Monitor unit and dose calculation were performed using TPS.

The multi-leaf collimator (MLC) conformed to the whole brain's shape, which was 3 cm away from the brain. However, the MLC was decreased to 1 cm from the brain since the 3 cm was too big (Orton et al. 2017). As for the dose volume histogram (DVH) analysis, the prescribed dose was already less than 25 Gy, which was lower than the tolerance limit of most OARs. The algorithm used in this planning was the Collapse Cone algorithm. 6 MV photon beam was used for phantom characterization using GafChromic EBT-XD films, TLD and OSL dosimeter. The plan was then exported to the LINAC through the ARIA system in DICOM (Digital Imaging and Communications in Medicine) RT format.

The respective head and neck treatment planning of the RANDO® RP was applied to the CT-simulation image of the 3D-printed RP. Then, a new parallel-opposed right and left lateral beam was planned on the 3D-printed RP. First, the 3D-printed RP undergoes the image registration process with a new plan target volume (PTV), which comprises the shape of the whole brain. After that, the parallel-opposed beam comprehends the right lateral and left lateral beams were applied. Finally, the MLC confirmed the shape of the PTV with the isocentre.

After finishing the plan, a dose of 400 cGy was prescribed to the phantom, and then a dose calculation was performed. The live dose at 95% isodose white line was viewed to contemplate the plan target area coverage, and since the 95% isodose line shows the coverage of all the PTV areas, the treatment evaluation was approved through the plan. The plan was exported to the ARIA system in DICOM RT format.

Calibrations of EBT-XD films

This study used EBT-XD GafChromic™ films (Ashland Advanced Materials, Bridgewater, NJ). Before accomplishing the phantom dosimetry assessment using films, the calibration was first conducted using four films with 2 cm × 2 cm measurements. The calibration setup was based on the standard regulations by AAPM (The American Association of Physicist in Medicine) (Niroomand-Rad et al. 1998). First, each film was marked with an upward arrow for the same film orientation during scanning and irradiation (Howard, Herman & Grams 2020). Then, the 16 cm solid water phantom was used with standard parameters, 10 cm × 10 cm field size, film located at D_{max} (1.5 cm from the surface of the solid water phantom), and 100 cm source-to-surface distance (SSD). The calibration doses were implemented in 0 to 10 Gy of 6 MV photon energy.

After 24 h, the film scanning and readings were conducted using the EPSON Flatbed scanner 10000 XL expression (EPSON, USA), FilmScan software, and PTW FilmCal 2.4 software (PTW-Freiburg, Freiburg, Germany). The orientation of all films during the irradiation and scanning process was symmetrical (Howard, Herman & Grams 2020). The pre-calibration curve was saved as a calibration table for dose determination. The optical density (OD) was calculated using Equations (1) and (2) (Devic et al. 2005), and the linear graph of OD versus the prescribed dose was constructed. The graph of net optical density per unit absorbed dose versus prescribed dose was constructed (Andres et al. 2010; Arjomandy et al. 2010; Borca et al. 2013; Niroomand-Rad et al. 1998).

$$Optical\ density\ (OD) = \log\left(\frac{I_0}{I}\right) \quad (1)$$

$$net\ OD = OD_{exp} - OD_{unexp} = \log\left(\frac{I_{unexp}}{I_{exp}}\right) \quad (2)$$

where I_0 is the initial intensity; I is the intensity transmitted through the film; *exp* is the exposed film; and *unexp* is the unexposed film.

Calibrations of TLD

The 3 × 3 × 1 mm^3 of TLD-100 (Radiation Products Design, Inc.), composed of lithium fluoride doped with magnesium and titanium (LiF: Mg, Ti; TLD chips), were employed. The application of TLDs started with three processes: (1) a pre-irradiation process called the annealing process, (2) irradiation, and (3) a readout process. First, TLDs were prepared by undertaking a sensitivity test by heating the TLDs at 400 °C for one hour and 100 °C for the next 2 h using a TLD Programmable Annealing Oven (model: PTW TLD 321/t/100). Then, the TLDs were cooled for 1 h to erase the residual signal from the previous irradiation. After that, the TLDs were placed in a plastic water irradiation plate designated specifically for TLD chips for irradiation at a standard calibration setup with 6 MV photon energy. After irradiation, the TLD chips were left for 24 h.

When reaching 1 to 2 h before the reading takes place, an extra precaution in the sensitivity accuracy was done by pre-heating the TLDs to maximize the elimination of the fading effect of LiF: Mg, Ti (Chen et al. 2010; Izak-Biran et al. 1996). First, the reading was started by taking a reading of the three photo-multiplier tubes (PMT) tests: noise test, light test, and background noise test. Next, the value of machine temperature and nitrogen gas pressure was recorded as machine quality assurance in TLD reading steps. Then, the readings were substantially accepted for the following reading action from the TLD reader (Harshaw, model 3500). Finally, all 89 TLD chips were read out, and a selection of golden and less-sensitive chips

was determined. The golden TLDs were chosen based on their standard calculation error value of ± 5% (Molineu et al. 2005) as dosimeters for RANDO® RP and 3D-printed RP.

Calibrations of OSLD

The OSLD nanoDot was calibrated using a PRIMUS linear accelerator with 6 MV photon energy. The OSL nanoDot dosimeter was exposed at source to surface distance (SSD) at 100 cm, maximum depth (D_{max}) at 1.5 cm, field size 10 cm × 10 cm, and depth 10 cm. OSLD was placed between 1.5 cm bolus and 10 cm of the solid water phantom. Ten dosimeters were irradiated with a dose ranging from 50 cGy to 600 cGy, with two dosimeters kept as the control for background measurement. The measurement of the OSLD was carried out using the microSTAR® Dosimetry System and Reader (Landauer, France) at Nuclear Agency Malaysia.

After obtaining the reading, the OSL nanoDot dosimeters were annealed using an annealer for 24 h to reduce the reading and to be used again for absorbed dose measurement in the phantom. The result of OSL nanoDot dosimeters was presented as a calibration curve of OSL signal against absorbed dose (in cGy). The absorbed dose was calculated using Equation (3). The linear equations and determination coefficient (R^2) were determined.

$$Dose = \frac{PMT\ counts}{Calibration\ \text{factor} \times \text{Sensitivity}} \quad (3)$$

where the dose is the reference dose at the same condition as OSLD; PMT counts are the number of photons created by the PMT; the calibration factor is used to calculate the dose from OSLD; and sensitivity is the sensitivity of OSLD (Yusuf et al. 2014).

CHARACTERIZATION OF 3D-PRINTED HEAD RP WITH EBT-XD FILMS

Optimization of the films' shape was conducted. The EBT-XD GafChromic films were prepared according to the phantom slice's surface. Four films were placed between slices 1 and 5. The 3D-printed RP has also been wrapped entirely using sticky cellulose tape to reduce the air gap.

Afterward, the phantoms were placed on a treatment couch with the help of an immobilization device, head-rest type A (for RANDO® RP), head-rest type B (for 3D-printed RP), and 1 cm of poly-B for better positioning. The position of the phantom was aligned on a treatment couch with the help of a laser from the midline, right, and left lateral. Then, the treatment couch's lateral, longitudinal, and vertical angles were adjusted based on the isocenter of the phantom. The gantry was rotated to the right lateral of the phantom at 270°, and the RANDO® RP was ready to be irradiated. The setup and positioning of the 3D-printed head phantom with all the isocentre and laser intersections were similar to the RANDO® RP. Finally, the phantoms were irradiated with a single fraction of 400 cGy of 6 MV photon energy using LINAC. After 24 h of irradiation, the films were scanned using EPSON Flatbed Scanner and the gamma index were analyzed using Verisoft 5.1 software.

Gamma index evaluation with standard shape phantom has become a standard technique to compare measured and calculated dose distribution using commercial radiation TPS (Kadoya et al. 2019). The gamma analysis was done on the exposed films in both phantoms from 1 mm distance-to-agreement with a 1% dose difference until 5 mm distance-to-agreement with a 5% dose difference for the maximum dose of a measured slice is 400 cGy. The analysis was also set to a 5.0% dose difference for values below 100 cGy. The passing criteria of the gamma index must be less than and equal to 1.0 between the film's measurement plane and the treatment plan's reference plane, with the green area corresponding to 90% to 100% of the point dose. The yellow area indicates a point dose match between 75% and 90%, whereas the red area indicates a failed point dose match between 0% and 75%. The standard gamma index was < 1 with 3 mm of distance-to-agreement and 3% of dose difference with passing criteria of 90% to 100% (Gracia-Garduno et al. 2014; Ju et al. 2010; Kadoya et al. 2019).

CHARACTERIZATION OF 3D-PRINTED HEAD RP WITH TLD

The last vestigial 40 TLD chips were used and inserted into the slots in 3D-printed head and RANDO® RPs. Finally, the head and neck treatment planning with the whole brain target area was applied for the irradiations with a single fraction of 400 cGy of 6 MV photon beam energy. The absorbed dose and TL signals were calculated.

CHARACTERIZATION OF 3D-PRINTED HEAD RP WITH OSL

Due to limitations with dosimetry placement inside the RANDO® RP, only the 3D-printed head phantom was irradiated with OSLD nanoDot. The OSLD were placed into slots inside the 3D-printed head phantom in slices 2, 3, 4, and 5. The contouring of the brain target area was used to determine these slots. Each slot was 1.5 cm × 1.5 cm in dimension. Blu-tack adhesive was used to cover the air gaps around the OSL nanoDot dosimeter within the slot. Then, the phantom was wrapped using adhesive tape to keep the slices close together to reduce the air gaps. The phantom was irradiated with 6 MV photon energy.

The OSL nanoDot dosimeters were read using microSTAR® Dosimetry System and Reader (Landauer, France) at Malaysian Nuclear Agency. The reader consists of an array of green light-emitting diodes (LEDs) as a high-intensity stimulating source and works in continuous-wave OSL mode to measure the OSL signal (Musa et al. 2017). The raw deep dose was then subtracted from the initial deep dose to obtain the actual deep dose of the OSL nanoDot dosimeter, as shown in Equation (4).

$$Actual\ deep\ dose\ of\ OSL\ (cGy) = Raw\ deep\ dose - Initial\ deep\ dose \quad (4)$$

The percentage dose difference (DD%) was calculated using Equation (5) to compare the difference between OSL measurement and calculated dose in the treatment plan and OSL measurement and TLD measurement.

$$DD\ \% = \frac{OSL\ measurement\ -\ calculated\ dose\ in\ TPS\ or\ TLD}{Point\ dose\ in\ TPS\ or\ TLD} \times 100 \quad (5)$$

RESULTS

GEOMETRIC EVALUATION OF 3D-PRINTED HEAD PHANTOM

As demonstrated in Figure 2, a few characteristics possessed by the phantom is that it was produced in 9 slices, excluding the top slice following the same structures as the standard RANDO® RP. The facial features of the printed phantom are similar to the RANDO® RP's features. Each slice of the 3D-printed RP is assumed to be printed grossly identical to the RANDO® RP. The difference in the 3D-printed phantom was that each slot was bigger (10 mm^2) compared to the RANDO® RP's (1.25 mm^2). On the other hand, the depth of slots in the 3D-printed phantom is shallower (2.5 mm) than the RANDO® RP (25 mm) across the thickness of a slice. The total weight percentage difference is 15%. Each slice of the 3D-printed head phantom is heavier than the RANDO® RP's, except for the top slice.

CT NUMBER (HOUNSFIELD UNIT) ANALYSIS

Figure 3 shows the 3D-printed head RP that went through the CT scan. The Hounsfield Unit (HU) or CT number measurement was completed in triplicate by plotting three regions of interest (ROIs) on each slice of the 3D-printed RP as shown in Table 1. The top slice and slice 1 were recorded with 106.5 and 107.2 HU, while for other slices, the HU is between 30 and 82 HU ranges. Meanwhile for RANDO® RP, the average HU values for air, bone and tissue are -931,1168 and 20 respectively for different region and slices (Thomas et al. 2009).

DOSIMETRY CHARACTERIZATION USING GAFCHROMIC EBT-XD FILMS

After 24 h of irradiation, four Gafchromic EBT-XD films were scanned, the lookup table was used and the pre-calibration curve was applied, and the gamma analysis was conducted. Table 2 shows the result of gamma analysis for the exposed film with RANDO® RP and 3D-printed head phantom with the treatment plan. The gamma analysis of Gafchromic EBT-XD films with the treatment plan of RANDO® RP was between 71.50% and 75.53% for 1%/1 mm until 5%/5 mm of DD/DTA criteria. For exposed EBT-XD films under 3D-printed head phantom with the treatment plan, the result of gamma analysis was between 59.78% and 67.15%. Furthermore, all four films under the RANDO® head phantom have a 100% green area of passing criteria at 42%/42 mm, indicating a 42% dose difference between exposed films and the treatment plan. On the other hand, the five criteria of DD/DTA for films 1, 2, and 3 were under the red region. Only film 4 of 5%/5 mm criteria fell under the yellow region. However, the green area of passing rate of gamma analysis of EBT-XD films fell at 30%/30 mm of DD/DTA. The gamma analysis for film 2 (located between slices 2 to 3) from both RPs is shown in Figure 4.

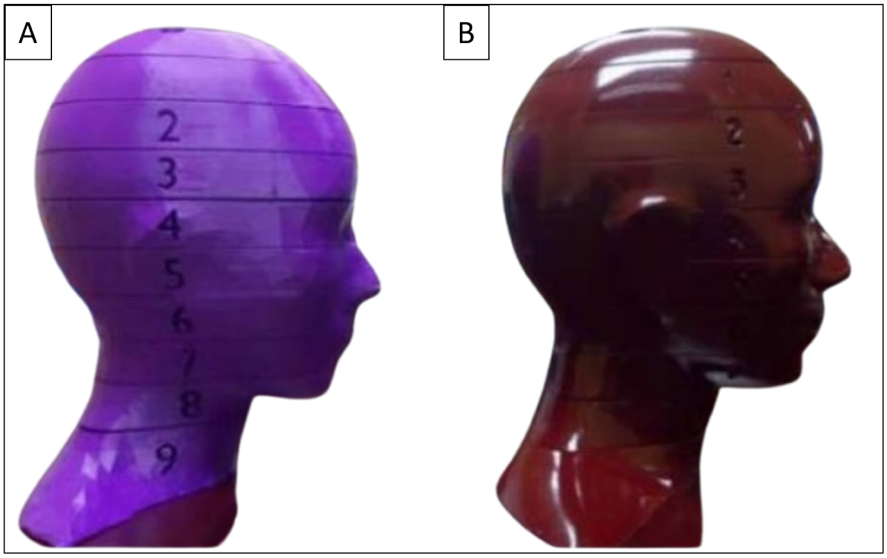

FIGURE 2. Side-by-side comparison of the: (A) 3D-printed head RP, (B) RANDO® RP

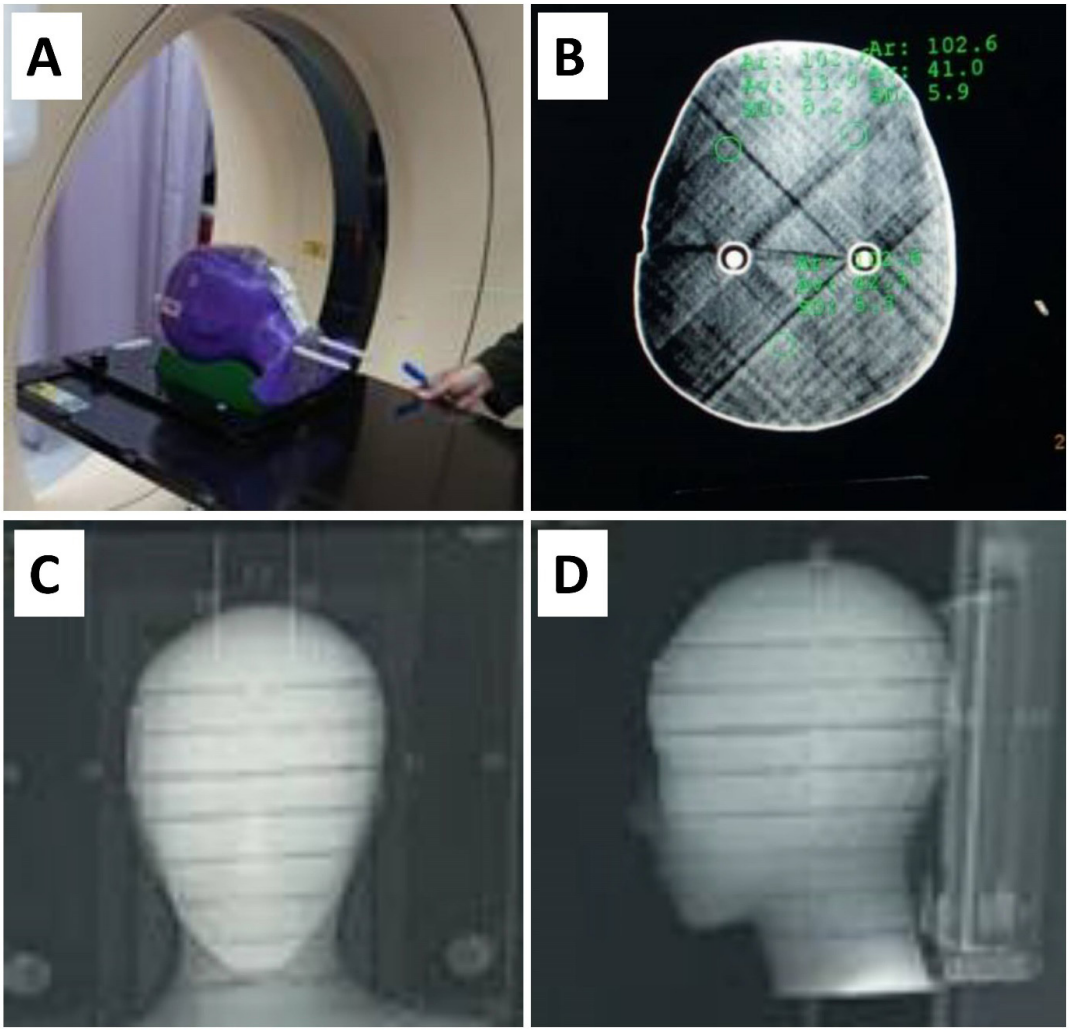

FIGURE 3. Verifying the imaging effect of the 3D-printed head phantom: (A) CT scanning of the phantom, (B) HU measurement of slice 3, (C) frontal view of CT image, and (D) lateral view of CT image

TABLE 1. Average HU number of the 3D-printed head phantom's slices

Slice	HU number ± SD
Top	106.5 ± 12.5
1	107.2 ± 7.7
2	81.0 ± 8.8
3	35.7 ± 6.5
4	42.2 ± 7.0
5	26.1 ± 5.8
6	45.9 ± 5.9
7	61.5 ± 5.5
Average	63.3 ± 31.6

HU, Hounsfield units; SD, standard deviation

TABLE 2. The average percentage of dose difference/dose-to-agreement (DD/DTA) from the gamma analysis of EBT-XD films

Gamma criteria	RANDO® RP	3D-printed RP
1%/1 mm	71.50%	59.78%
2%/2 mm	72.28%	61.43%
3%/3 mm	73.10%	63.30%
4%/4 mm	74.28%	65.20%
5%/5 mm	75.53%	67.15%
30%/30 mm	n/a	99.50%
42%/42 mm	100.00%	n/a

n/a, Not Applicable; RP, radiotherapy phantom

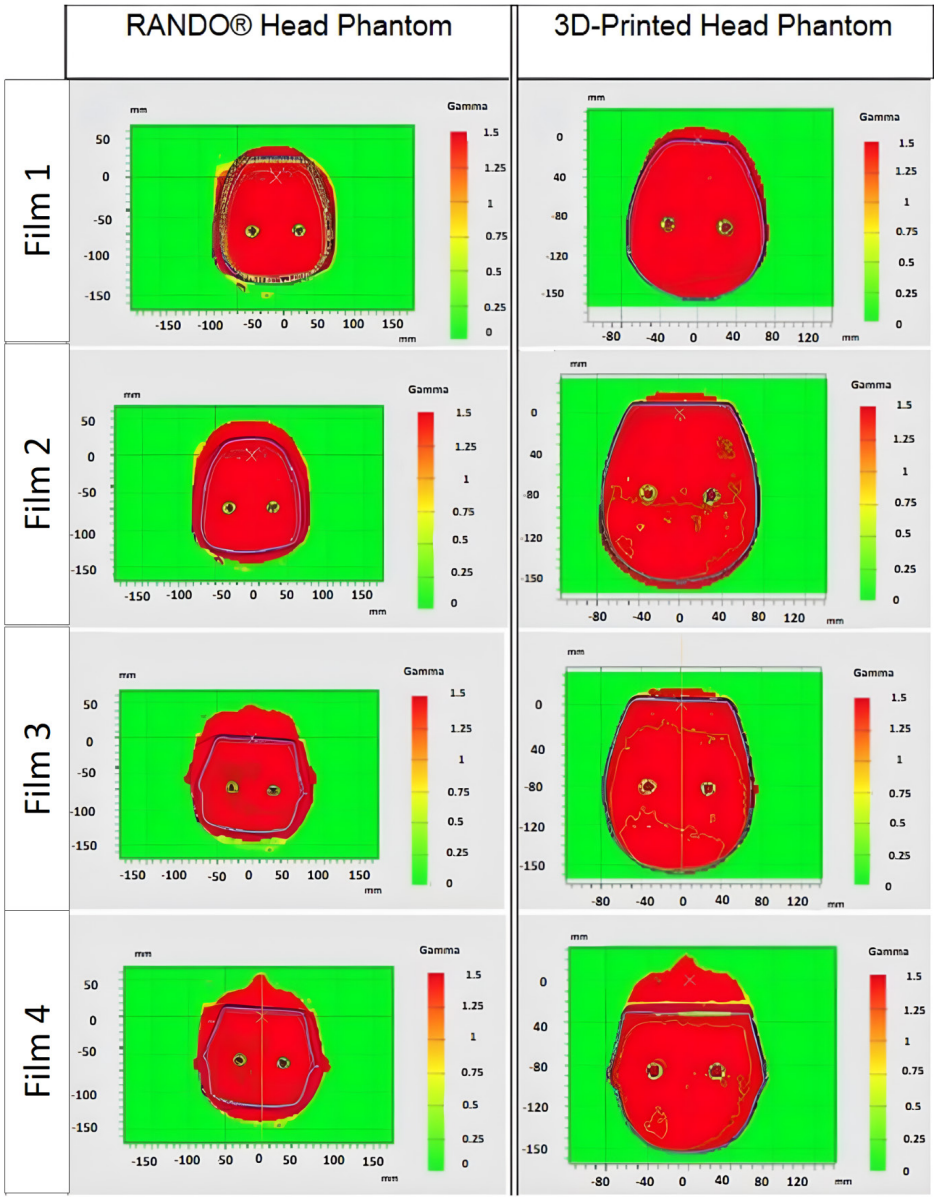

FIGURE 4. Comparison of gamma index for both RANDO® RP and 3D-printed RP at location between slice 1 and two for Film 1, between slice 2 and 3 for Film 2, between slice 3 and 4 for Film 3 and between slice 4 and 5 for Film 4, respectively

DOSIMETRY CHARACTERIZATION USING TLD

The irradiation was performed with head and neck treatment planning with a dose of 400 cGy as recommended (Salmanian et al. 2018). The average absorbed dose captured by the TLDs within 3D-printed head RP was 99% similar to that of TPS and RANDO® RP, which was 415.58 cGy as presented in Figure 5. Besides, the average of TL signals for 3D-printed head RP was 62.34 μC, which was approximate to the TL signals for RANDO® RP (60.28 μC). The dosimetry evaluation using TLD of the 3D-printed head phantom and RANDO® RP is almost equivalent to the measured dose value. The result obtained from TLD in 3D-printed head phantom is within 99% as acquired by TLD in standard RANDO® RP.

DOSIMETRY CHARACTERIZATION USING OSLD

After irradiation, the OSL nanoDot dosimeters were analyzed to assess the absorbed dose. The average actual dose of OSL was 438.37 cGy with 293550.20 PMT counts. The prescribed dose for irradiating 3D-printed head phantom for the right and left lateral beam of head and neck treatment was a single fraction of 400 cGy, whereas the calculated dose from TPS was 405.40 cGy. However, it shows that the prescribed dose is lower than the calculated dose (438.37 cGy). Comparisons were also made with the other dosimeters measured doses from TPS and TLD (415.58 cGy). The percentage dose difference (DD%) values among the dosimeters are stated in Table 3.

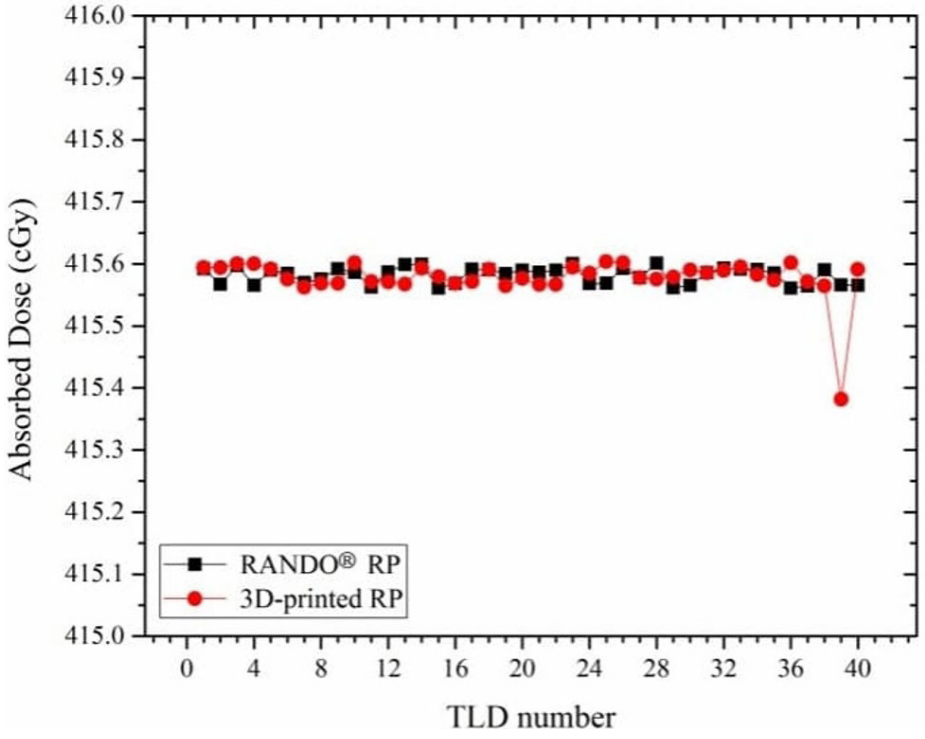

FIGURE 5. TLD readings for both RANDO® and 3D-printed RPs, measured in cGy

TABLE 3. Percentage dose difference (DD%) measurement of the 3D-printed RP using different dosimeters

Compared dosimeters	DD%
TPS – TLD	< 1%
TPS – OSL	8.1%
TPS – EBT-XD	30%
OSL – TLD	5.48%

RP, radiotherapy phantom

DISCUSSIONS

Geometric evaluation of 3D-Printed head phantom demonstrated the slice error values of within the 1 mm to 42 mm fluctuation range throughout the ten slices. However, the average slice measurement errors with standard deviation (SD) calculated are 0.48% ± 10.02% for x-values and 6.24% ± 13.19% for y-values. The editing process of the 3D-printed RP also somewhat increased its size. The rendering and smoothing of the 3D-printed RP's outer part involved adding up and reducing the surface volume of the printed phantom (Craft & Howell 2017). Nevertheless, the 3D-printed RP is grossly in the same shape as the RANDO® RP when compared side-by-side. The difference in the weightage of the slices might be due to the bigger size of the 3D-printed RP than the RANDO® RP. Besides, it is assumed that the 100% infill PLA used for the 3D-printed RP was heavier than the RANDO® RP's. A clear-PLA was also found to have 20% higher physical density than water (Burleson et al. 2015). The multi-densities of the RANDO® RP could not be simulated during the 3D scanning. Thus, the produced 3D-printed head RP is homogeneous inside and earned more weight. The weight of the 3D printed phantom is somehow become limitation especially during treatment positioning where the phantom tends to fall apart in horizontal position and cause the air gap that might affect the dosimetric results especially for measurement with GafChromic films™.

Moreover, the CT number analysis estimated for slices 3 to 6 are similar to the HU of white matter (HU = 20 to 30), muscle and soft tissue (HU = 20 to 40), gray matter (HU = 30 to 40), and blood (HU = 65 to 100) (Kamalian, Lev & Gupta 2016; Karla 2018; Lev & Gonzalez 2002). A new head and neck RP work deduced that PLA could also substitute a spongy bone (Ahmadi et al. 2021). The average HU value for the 3D-printed RP is 63.3 ± 31.6 HU. A study on a patient-specific 3D-printed head and neck PLA bolus reported that their attained average HU was 160 (Burleson et al. 2015). However, a later PLA head phantom study by Kamomae et al. (2017) gained less average HU, which was −6 ± 18 HU. HU number discrepancies can be caused by many factors, such as the type of 3D printers and software utilization (Kamomae et al. 2017), material's properties that could induce thermal warping during the printing process (Kamomae et al. 2017), interference of the air gap between the material's fill density (Madamesila et al. 2016), and techniques and RP's positioning during the CT simulation (Burleson et al. 2015). The PLA is determined to be tissue equivalence to solid water by Bustillo, Tumlos and Remoto (2019) in which the mean relative electron density, ρe, w, and mass density, ρ (g/cm3), are 0.988 and 0.99, respectively. PLA also has better properties for radiology than other materials, such as ABS (Burleson et al. 2015; Kamomae et al. 2017). PLA is considered advisable to replace solid water phantoms in radiotherapy because the dose errors measured in both phantoms are less than or within the 5% tolerance value (Zain et al. 2019). Different density infills of PLA materials and their relationship with the air gap or infill-to-density characteristic were studied, and their uniformity for dosimetric quality assurance purposes was proven (Madamesila et al. 2016; Zain et al. 2019).

Dosimetry evaluation have been performed using GafChromicTM EBT-XD films, thermoluminescence dosimeter (TLD-100), and NanoDot optically stimulated luminescence dosimeter (OSLD). The choice of the dosimeter is justified due to their characteristic as point (TLD-100 and OSLD) and 2 Dimension (2D) dosimeter (films) that can be easily position within both phantoms. These three types of dosimeters also commonly used and reliable to provide accurate radiotherapy dose verification and comprehensive dosimetry. The results show that the percentage of 59.78% to 67.15% for 1%/1 mm until 5%/5 mm of DD/DTA criteria from the gamma analysis of 3D-printed head phantom were observed for the dosimetry characterization using GafChromic EBT-XD films. In a previous study, developing a low-cost and customized anthropomorphic thoracic phantom slab using PLA material study produced around 5%/1 mm gamma criterion, which demonstrated a good agreement in a range of 90.2% to 98% for comparison between EBT3 films and treatment plan (Tino et al. 2022). Another research utilized the 3%/3 mm criterion and demonstrated an excellent agreement for all areas of the 3D-printed RP at 96.1% (Kadoya et al. 2019). Therefore, it is concluded that developing a novel 3D-printed RP made up of PLA material can be used in the dose verification of patient-specific quality assurance (Kadoya et al. 2019; Tino et al. 2022). In this study, the DD% between the phantoms and the treatment plan was rather significant, indicating that there may have been an element of uncertainty. Another hollow head and neck phantom with inserts found that the 5%/4 mm pass rate obtained by different TPS, such as XiO, Pinnacle^3, Eclipse, and TomoTherapy, were 54%, 56%, 72%, and 79%, respectively (Molineu et al. 2013). Thus, the current work's 5%/5 mm gamma criterion of 67.15% for the 3D-printed RP is acceptable. In addition, the air gaps between the phantoms and the handling of films during the irradiations might cause uncertainty (Radaideh et al. 2013). Therefore, the films should be handled appropriately according to the guidelines of AAPM Task Group No. 55 (Niroomand-Rad et al. 1998; Rivard et al. 2004; Soares, Trichter & Devic 2009). In this study, the holes are made at the film's center for the phantom's stick using a cutter blade. Therefore, it may affect the film's surface and increase the fingerprints and smudges, affecting its analysis. During the measurement, the GafChromic™ EBT-XD films were sandwiched in between the phantom's slices which somehow cause unnecessary air gap that influence the dose reading. In the case of films dosimetry using these types of phantoms, improvise technique is required to achieve more accurate results.

Additionally, the average absorbed dose captured by the TLDs within 3D-printed head RP was 99% similar to that of TPS and RANDO® RP. The average point-by-point standard error of both RPs was 2.9% to 3.6%, in agreement with another head and neck phantom study (Radaideh et al. 2012). The errors were also lower than the 5% deviations found in TLD-100 when the dose approached 300 cGy (Harris et al. 1997). Besides, the average of TL signals for 3D-printed head RP was approximate to the TL signals for RANDO® RP. The uniformity of the PLA density according to this result is verified in terms of radiation dosimetry since the input and output of the dose given were 99% similar (Bentz et al. 2016; Chen et al. 2010; Izak-Biran et al. 1996; Murthy 2013). Hence, with those standard matching results, this economic 3D-printed RP was proven to be equivalent in density, and this condition served the phantom suitable to be used in radiotherapy radiation dosimetry.

Apart from that, the OSL nanoDot dosimeters were also analyzed to assess the absorbed dose. Different treatment plans might cause the uncertainty resulting from these percentage dose differences of TPS, even though the same dose of 400 cGy per fraction was prescribed. These uncertainties also might be caused by the air gap error between the 3D-printed head phantoms. Aside from that, the placement of OSL inside the slot of the 3D-printed head phantom's slice, which is coated with blue-tack adhesive, might also contribute to a minor error in OSL measurement. Nevertheless, a multi-institutional clinical trial of the head and neck phantom found that even 33 irradiation sessions failed TLD and film dosimetric criteria (Molineu et al. 2013). They concluded that the phantom's irradiation pass rates depended on the delivery types, TPS, linear accelerators, and their combinations (Molineu et al. 2013). This indicate performance of the phantom need to be improved in term of their physical dimension and geometric design, tissue equivalent materials and dosimetric capabilities.

CONCLUSION

The anthropomorphic head phantom was successfully developed using Kinect® Xbox 360® scanner with the 3D-printed fabrication. The fabricated phantom's geometrical shape and contour are grossly similar to the RANDO® RP. The dosimetry characterization of the 3D-printed head phantom was appropriately compared with the standard RANDO® RP. CT number analysis discovered that the 100% infill of PLA could mimic soft tissues, muscles, white matter, gray matter, and blood. The GafChromic™ EBT-XD films showed a 100% pass rate at 30%/30 mm criteria. On the other hand, dose measurement using TLD resulted in 99% similarity compared to RANDO® RP. The TPS – OSL and OSL - TLD comparisons only showed 5% to 8% uncertainty. Hence, the 3D-printed head phantom is tested to be applicable for clinical radiotherapy dosimetry even though full dosimetry benefits are not yet achievable compared to the standard RANDO® RP. In future work, further optimization is required to achieve a fully functioning patient-specific radiotherapy phantom. In summary, newly developed phantom should replicate patient specific tissue heterogeneity and anatomical structures as well as tailored to individual patients using imaging data such as CT and MRI while application of surface scanner may enhance phantom superficial anatomical features in complex region such as head and neck.

ACKNOWLEDGEMENTS

The authors thank the Ministry of Higher Education, Malaysia for Prototype Research Grant Scheme with Project Code: (PRGS/2/2019/TK04/UKM/02/1) and Geran Galakan Penyelidik Muda GGPM-2023-068. The authors acknowledged the Malaysian Nuclear Agency and their staff for providing access to the OSL nanodot dosimeter reader.

REFERENCES

Ahmad, M.A., Mustaza, S.M., Mokri, S.S., Azmi, N.A., Ahmad, R., Ramli, R., Rahman, W.N.W.A. & Abd Rahni, A.A. 2021. Development of a 3D printed motion mechanism for a 4D respiratory motion phantom. *2020 IEEE-EMBS Conference on Biomedical Engineering and Sciences (IECBES)*. pp. 132-135. DOI: 10.1109/IECBES48179.2021.9398831

Ahmadi, M., Ramezani, A.M., Hariri, T.S. & Azma, Z. 2021. Manufacturing and evaluation of a multi-purpose Iranian head and neck anthropomorphic phantom called MIHAN. *Medical & Biological Engineering & Computing* 59: 1611-1620. https://doi.org/10.1007/s11517-021-02394-y

Alssabbagh, M., Tajuddin, A.A., Abdul Manap, M.b. & Zainon, R. 2017. Evaluation of nine 3D printing materials as tissue equivalent materials in terms of mass attenuation coefficient and mass density. *International Journal of Advanced and Applied Sciences* 4(9): 168-173. https://doi.org/10.21833/ijaas.2017.09.024

Alzahrani, M., O'Hara, C., Bird, D., Baldwin, J.P., Naisbit, M., Teh, I., Broadbent, D.A., Al-Qaisieh, B., Johnstone, E. & Speight, R. 2024. Optimisation of cone beam CT radiotherapy imaging protocols using a novel 3D printed head and neck anthropomorphic phantom. *Physics in Medicine & Biology* 69(21). DOI 10.1088/1361-6560/ad88d2

Andres, C., Del Castillo, A., Tortosa, R., Alonso, D. & Barquero, R. 2010. A comprehensive study of the Gafchromic EBT2 radiochromic film. A comparison with EBT. *Medical Physics* 37(12): 6271-6278. https://doi.org/10.1118/1.3512792

Arjomandy, B., Tailor, R., Anand, A., Sahoo, N., Gillin, M., Prado, K. & Vicic, M. 2010. Energy dependence and dose response of Gafchromic EBT2 film over a wide range of photon, electron, and proton beam energies. *Medical Physics* 37(5): 1942-1947. https://doi.org/10.1118/1.3373523

Attix, F.H. 2004. *Introduction to Radiological Physics and Radiation Dosimetry.* KGaA, Weinheim: Wiley-VCH Verlag GmbH & Co.

Babaloui, S., Jafari, S., Polak, W., Ghorbani, M., Hubbard, M.W., Lohstroh, A., Shirazi, A. & Jaberi, R. 2020. Development of a novel and low-cost anthropomorphic pelvis phantom for 3D dosimetry in radiotherapy. *Journal of Contemporary Brachytherapy* 12(5): 470-479. https://doi.org/10.5114/jcb.2020.100380

Borca, V.C., Pasquino, M., Russo, G., Grosso, P., Cante, D., Sciacero, P., Girelli, G., Porta, M.R.L. & Tofani, S. 2013. Dosimetric characterization and use of GAFCHROMIC EBT3 film for IMRT dose verification. *Journal of Applied Clinical Medical Physics* 14(2): 158-171. https://doi.org/10.1120/jacmp.v14i2.4111

Burleson, S., Baker, J., Hsia, A.T. & Xu, Z. 2015. Use of 3D printers to create a patient-specific 3D bolus for external beam therapy. *Journal of Applied Clinical Medical Physics* 16: 166-178. https://doi.org/10.1120/jacmp.v16i3.5247

Bentz, B.Z., Chavan, A.V., Lin, D., Tsai, E.H. & Webb, K.J. 2016. Fabrication and application of heterogeneous printed mouse phantoms for whole animal optical imaging. *Applied Optics* 55(2): 280-287. https://doi.org/10.1364/AO.55.000280

Bogmis, A.I., Popa, A.R., Adam, D., Ciocâltei, V., Guraliuc, N.A., Ciubotaru, F. & Chiricuță, I.C. 2020. Complex target volume delineation and treatment planning in radiotherapy for malignant pleural mesothelioma (MPM). *International Journal of Medical Physics, Clinical Engineering and Radiation Oncology* 9(3): 125-140. DOI: 10.4236/ijmpcero.2020.93012

Bustillo, J.P., Tumlos, R. & Remoto, R.Z. 2019. Intensity Modulated Radiotherapy (IMRT) phantom fabrication using Fused Deposition Modeling (FDM) 3D printing technique. *World Congress on Medical Physics and Biomedical Engineering 2018*. Singapore: Springer. pp. 509-515.

Bustillo, J.P.O., Posadas, J.R.D., Mata, J.L., Inocencio, E.T., Rosenfeld, A.B. & Lerch, M.L.F. 2024a. 3D printed heterogeneous paediatric head and adult thorax phantoms for linear accelerator radiotherapy quality assurance: From fabrication to treatment delivery. *Biomedical Physics & Engineering Express* 10(5): 055037. DOI 10.1088/2057-1976/ad6f13

Bustillo, J.P.O., Paino, J., Barnes, M., Cayley, J., de Rover, V., Cameron, M., Engels, E.E., Tehei, M., Beirne, S., Wallace, G.G. & Rosenfeld, A.B., 2024b. Design, construction, and dosimetry of 3D printed heterogeneous phantoms for synchrotron brain cancer radiation therapy quality assurance. *Physics in Medicine & Biology* 69(14): 145003. DOI 10.1088/1361-6560/ad5b48

Craft, D.F. & Howell, R.M. 2017. Preparation and fabrication of a full-scale, sagittal-sliced, 3D-printed, patient-specific radiotherapy phantom. *Journal of Applied Clinical Medical Physics* 18: 285-292. https://doi.org/10.1002/acm2.12162

Chen, C.Y., Liu, K.C., Chen, H.H. & Pan, L.K. 2010. Optimizing the TLD-100 readout system for various radiotherapy beam doses using the Taguchi methodology. *Applied Radiation and Isotopes* 68: 481-488. https://doi.org/10.1016/j.apradiso.2009.12.001

Dawood, A., Marti, B.M., Sauret-Jackson, V. & Darwood, A. 2015. 3D printing in dentistry. *British Dental Journal* 219: 521-529. https://doi.org/10.1038/sj.bdj.2015.914

Devic, S., Seuntjens, J., Sham, E., Podgorsak, E.B., Schmidtlein, C.R., Kirov, A.S. & Soares, C.G. 2005. Precise radiochromic film dosimetry using a flat-bed document scanner. *Medical Physics* 32(7 Part1): 2245-2253. https://doi.org/10.1118/1.1929253

DeWerd, L.A. & Kissick, M. 2014. *The Phantoms of Medical and Health Physics*: *Devices for Research and Development.* Berlin: Springer;

Ehler, E.D., Barney, B.M., Higgins, P.D. & Dusenbery, K.E. 2014. Patient specific 3D printed phantom for IMRT quality assurance. *Physics in Medicine & Biology* 59: 5763-5773. https://doi.org/10.1088/0031-9155/59/19/5763

Frigo, S.P. 2014. Radiation therapy dosimetry phantoms. In *The Phantoms of Medical and Health Physics*: *Devices for Research and Development*, edited by DeWerd, L.A. & Kissick, M. New York: Springer Science Business Media. pp. 17-38.

García-Garduño, O.A., Rodríguez-Ponce, M., Gamboa-deBuen, I., Rodríguez-Villafuerte, M., Galván De La Cruz, O.O. & Rivera-Montalvo, T. 2014. Effect of dosimeter type for commissioning small photon beams on calculated dose distribution in stereotactic radiosurgery. *Medical Physics* 41(9): 092101. https://doi.org/10.1118/1.4892176

Gear, J.I., Cummings, C., Craig, A.J., Divoli, A., Long, C.D., Tapner, M. & Flux, G.D. 2016. Abdo-Man: A 3D-printed anthropomorphic phantom for validating quantitative SIRT. *EJNMMI Physics* 3: 17. https://doi.org/10.1186/s40658-016-0151-6

Harris, C.K., Elson, H.R., Lamba, M.A.S. & Foster, A.E. 1997. A comparison of the effectiveness of thermoluminescent crystals LiF:Mg,Ti, and LiF:Mg,Cu,P for clinical dosimetry. *Medical Physics* 24: 1527-1529. https://doi.org/10.1118/1.598042

Hoskin, P. & Alonzi, R. 2016. Imaging for radiotherapy planning. *Radiology Key.* https://radiologykey.com/imaging-for-radiotherapy-planning/. (Accessed on 10 Nov 2022).

Howard, M.E., Herman, M.G. & Grams, M.P. 2020. Methodology for radiochromic film analysis using FilmQA Pro and ImageJ. *PLoS ONE* 15: e0233562. https://doi.org/10.1371/journal.pone.0233562

Izak-Biran, T., Malchi, S., Shamai, Y. & Alfassi, Z.B. 1996. Low pre- and post-irradiation fading of LiF:Mg, Ti (TLD-100, TLD-600, TLD-700) using a preheat technique. *Radiation Protection Dosimetry* 64: 269-274. https://doi.org/10.1093/oxfordjournals.rpd.a031583

Jahnke, P., Schwarz, S., Ziegert, M., Schwarz, F.B., Hamm, B. & Scheel, M. 2019. Based 3D printing of anthropomorphic CT phantoms: Feasibility of two construction techniques. *European Radiology* 29: 1384-1390. https://doi.org/10.1007/s00330-018-5654-1

Ju, S.G., Han, Y., Kum, O., Cheong, K.H., Shin, E.H., Shin, J.S., Kim, J.S. & Ahn, Y.C. 2010. Comparison of film dosimetry techniques used for quality assurance of intensity modulated radiation therapy. *Medical Physics* 37(6Part1): 2925-2933. https://doi.org/10.1118/1.3395574

Kadoya, N., Abe, K., Nemoto, H., Sato, K., Ieko, Y., Ito, K., Dobashi, S., Takeda, K. & Jingu, K. 2019. Evaluation of a 3D-printed heterogeneous anthropomorphic head and neck phantom for patient-specific quality assurance in intensity-modulated radiation therapy. *Radiological Physics and Technology* 12: 351-356. https://doi.org/10.1007/s12194-019-00527-5

Kairn, T., Crowe, S.B. & Markwell, T. 2015. Use of 3D printed materials as tissue-equivalent phantoms. In *World Congress on Medical Physics and Biomedical Engineering 2015,* edited by Jaffray, D. IFMBE Proceedings. Toronto: Springer, Cham. pp. 728-731.

Kalra, A. 2018. Developing FE human models from medical images. In *Basic Finite Element Method as Applied to Injury Biomechanics*, edited by Yang, K.H. London: Elsevier. pp. 389-415. https://doi.org/10.1016/B978-0-12-809831-8.00009-X

Kamalian, S., Lev, M.H. & Gupta, R. 2016. Computed tomography imaging and angiography – principles. In *Handbook of Clinical Neurology.* edited by Masdeu, J.C. & González, R.G. Amsterdam: Elsevier B.V. pp. 3-20. https://doi.org/10.1016/B978-0-444-53485-9.00001-5

Kamomae, T., Shimizu, H., Nakaya, T., Okudaira, K., Aoyama, T., Oguchi, H., Komori, M., Kawamura, M., Ohtakara, K., Monzen, H. & Itoh, Y. 2017. Three-dimensional printer-generated patient-specific phantom for artificial *in vivo* dosimetry in radiotherapy quality assurance. *Physica Medica* 44: 205-211. https://doi.org/10.1016/j.ejmp.2017.10.005

Khan, F.M. 2014. Measurement of ionizing radiation. In *Khan's The Physics of Radiation Therapy*, 5th ed., edited by Khan, F.M. & Gibbons, J.P. Philadelphia: Lippincott Williams & Wilkins. p. 76.

Lev, M.H. & González, R.G. 2002. CT angiography and CT perfusion imaging. In *Brain Mapping: The Methods*, edited by Toga, A. & Mazziotta, J. 2nd ed. San Diego: Academic Press. pp. 427-484.

Madamesila, J., McGeachy, P., Villarreal Barajas, J.E. & Khan, R. 2016. Characterizing 3D printing in the fabrication of variable density phantoms for quality assurance of radiotherapy. *Physica Medica* 32: 242-247. https://doi.org/10.1016/j.ejmp.2015.09.013

Mann, P., Witte, M., Moser, T., Lang, C., Runz, A., Johnen, W., Berger, M., Biederer, J. & Karger, C.P. 2017. 3D dosimetric validation of motion compensation concepts in radiotherapy using an anthropomorphic dynamic lung phantom. *Physics in Medicine & Biology* 62(2): 573. DOI 10.1088/1361-6560/aa51b1

Molineu, A., Hernandez, N., Nguyen, T., Ibbott, G. & Followill, D. 2013. Credentialing results from IMRT irradiations of an anthropomorphic head and neck phantom. *Medical Physics* 40(2): 022101. https://doi.org/10.1118/1.4773309

Molineu, A., Followill, D.S., Balter, P.A., Hanson, W.F., Gillin, M.T., Huq, M.S., Eisbruch, A. & Ibbott, G.S. 2005. Design and implementation of an anthropomorphic quality assurance phantom for intensity-modulated radiation therapy for the Radiation Therapy Oncology Group. *International Journal of Radiation Oncology Biology Physics* 63(2): 577-583. https://doi.org/10.1016/j.ijrobp.2005.05.021

Mukwada, G., Hirst, A., Rowshanfarzad, P. & Ebert, M.A. 2024. Development of a 3D printed phantom for commissioning and quality assurance of multiple brain targets stereotactic radiosurgery. *Physical and Engineering Sciences in Medicine* 47(2): 455-463. https://doi.org/10.1007/s13246-023-01374-w

Musa, Y., Hashim, S., Karim, M.K.A., Bakar, K.A., Ang, W.C. & Salehhon, N. 2017. Response of optically stimulated luminescence dosimeters subjected to X-rays in diagnostic energy range. *Journal of Physics: Conference Series* 851(1): 012001. DOI 10.1088/1742-6596/851/1/012001

Murthy, K.V.R. 2013. Applications of TLDs in radiation dosimetry. *Defect and Diffusion Forum* 341: 211-230. https://doi.org/10.4028/www.scientific.net/DDF.341.211

Niroomand-Rad, A., Blackwell, C.R., Coursey, B.M., Gall, K.P., Galvin, J.M., McLaughlin, W.L., Meigooni, A.S., Nath, R., Rodgers, J.E. & Soares, C.G. 1998. Radiochromic film dosimetry: Recommendations of AAPM radiation therapy committee task group 55. *Medical Physics* 25(11): 2093-2115. https://doi.org/10.1118/1.598407

Oh, S.A., Kim, M.J., Kang, J.S., Hwang, H.S., Kim, Y.J., Kim, S.H., Park, J.W., Yea, J.W. & Kim, S.K. 2017. Feasibility of fabricating variable density phantoms using 3D printing for quality assurance (QA) in radiotherapy. *Progress in Medical Physic* 28(3): 106-110. https://doi.org/10.14316/pmp.2017.28.3.106

Orton, A., Gordon, J., Vigh, T., Tonkin, A. & Cannon, G. 2017. Differences in parotid dosimetry and expected normal tissue complication probabilities in whole brain radiation plans covering C1 versus C2. *Cureus* 9(5): e1217. doi: 10.7759/cureus.1217

Piperdi, H., Portal, D., Neibart, S.S., Yue, N.J., Jabbour, S.K. & Reyhan, M. 2021. Adaptive radiation therapy in the treatment of lung cancer: An overview of the current state of the field. *Frontiers in Oncology* 11: 770382. https://doi.org/10.3389/fonc.2021.770382

Park, J.W., Oh, S.A., Yea, J.W. & Kang, M.K. 2017. Fabrication of malleable three-dimensional-printed customized bolus using three-dimensional scanner. *PLoS ONE* 12: e0177562. https://doi.org/10.1371/journal.pone.0177562

Radaideh, K.M., Matalqah, L.M., Tajuddin, A.A., Lee, W.F., Bauk, S. & Munem, E.E.A. 2013. Development and evaluation of a Perspex anthropomorphic head and neck phantom for three dimensional conformal radiation therapy (3D-CRT). *Journal of Radiotherapy in Practice* 12(3): 272-280. doi:10.1017/S1460396912000453

Ramos, E. 2012. Kinect basics. *Arduino and Kinect Projects*. Berkeley: Apress. pp 23-34.

Rahman, M. 2017. *Beginning Microsoft Kinect for Windows SDK 2.0*. Berkeley: Apress.

Rahman, W.N., Abdul Razak, H., Sisin, N.N.T., Abdullah, R., Abdullah, A.N. & Rahni, A.A.A. 2023. Customized 3D-Printed TPU Slab Phantom for 6 MV Photon Beams Radiotherapy. *Proceedings of the 19th Asian Workshop on Polymer Processing (AWPP 2022). AWPP 2022. Springer Proceedings in Materials*, vol 24. Singapore: Springer. https://doi.org/10.1007/978-981-99-2015-0_7

Rivard, M.J., Coursey, B.M., DeWerd, L.A., Hanson, W.F., Saiful Huq, M., Ibbott, G.S., Mitch, M.G., Nath, R. & Williamson, J.F. 2004. Update of AAPM Task Group No. 43 Report: A revised AAPM protocol for brachytherapy dose calculations. *Medical Physics* 31(3): 633-674. https://doi.org/10.1118/1.1646040

Salmanian, S., Vaez Zade, V., Sanei, M. & Sharafi, A.A. 2018. The measurement of absorbed dose in thyroid, parathyroid, eye lens and gonads in radiotherapy of head and neck epithelial tumors by thermoluminescent dosimeter (TLD) method. *Frontiers in Biomedical Technologies* 5: 69-73.

Sands, G., Clark, C.H. & McGarry, C.K. 2023. A review of 3D printing utilisation in radiotherapy in the United Kingdom and Republic of Ireland. *Physica Medica* 115: 103143. https://doi.org/10.1016/j.ejmp.2023.103143

Steinmann, A., Alvarez, P., Lee, H., Court, L., Stafford, R., Sawakuchi, G., Wen, Z., Fuller, C.D. & Followill, D. 2020. MRIgRT head and neck anthropomorphic QA phantom: Design, development, reproducibility, and feasibility study. *Medical Physics* 47(2): 604-613. https://doi.org/10.1002/mp.13951

Soares, C.G., Trichter, S. & Devic, S. 2009. Radiochromic film. In *Clinical Dosimetry Measurements in Radiotherapy,* edited by Rogers, D.W.O. & Cygler, J.E. (2009 AAPM Summer School). AAPM, College Park. p. 1128.

Tagiling, N. 2019. Dosimetric characterisation of Gafchromic™ EBT3 films for nanoparticles-enhanced photon, electron, high dose rate 192-Ir and proton radiotherapy. MSc, Universiti Sains Malaysia (Unpublished).

Tino, R.B., Yeo, A.U., Brandt, M., Leary, M. & Kron, T. 2022. A customizable anthropomorphic phantom for dosimetric verification of 3D-printed lung, tissue, and bone density materials. *Medical Physics* 49(1): 52-69. https://doi.org/10.1002/mp.15364

Thomas, T.H.M., Devakumar, D., Purnima, S. & Ravindran, B.P. 2009. The adaptation of megavoltage cone beam CT for use in standard radiotherapy treatment planning. *Physics in Medicine & Biology* 54(7): 2067. DOI 10.1088/0031-9155/54/7/014

Yusuf, M., Saoudi, A., Alothmany, N., Alothmany, D., Natto, S., Natto, H., Molla, N.I., Mail, N., Hussain, A. & Kinsara, A.A. 2014. Characterization of the optically stimulated luminescence nanoDot for CT dosimetry. *Life Science Journal* 11(2): 445-450.

Zain, N.E. & Rahman, W.N. 2020. Three-dimensional (3D) scanning using Microsoft® Kinect® Xbox 360® scanner for fabrication of 3D printed radiotherapy head phantom. *Journal of Physics: Conference Series* 1497(1): 012005. DOI 10.1088/1742-6596/1497/1/012005

Zain, N.E.M., Jais, U., Abdullah, R. & Rahman, W.N.W.A. 2019. Dosimetric characterization of customized PLA phantom for radiotherapy. *Jurnal Sains Nuklear Malaysia* 31(2): 1-6.

Zhang, F., Zhang, H., Zhao, H., He, Z., Shi, L., He, Y., Ju, N., Rong, Y. & Qiu, J. 2019. Design and fabrication of a personalized anthropomorphic phantom using 3D printing and tissue equivalent materials. *Quantitative Imaging in Medicine and Surgery* 9(1): 94-100. doi: 10.21037/qims.2018.08.01

*Corresponding author; email: wnordiana@ukm.edu.my